Mathematical Biosciences and Engineering

MBE, 19(1): 394–419.
DOI: 10.3934/mbe.2022020
Received: 24 September 2021
Accepted: 31 October 2021
Published: 15 November 2021

http://www.aimspress.com/journal/MBE

Research article

Research on the control problem of actuator anti-saturation of supercavitating vehicle

Tao Bai* and Junkai Song

College of Intelligent Systems Science and Engineering, Harbin Engineering University, Harbin, 150001, China

* **Correspondence:** Email: baitao1@hrbeu.edu.cn.

Abstract: In the theoretical controller design of the high-speed supercavitating vehicle (HSSV), there will always be the problem that the physical saturation limit has to be exceeded by the motion range of the actuator to satisfy the requirements of stable motion of the supercavitating vehicle. This paper proposes a solution which could satisfy the requirements of stable motion of the vehicle without saturation of the actuator. First of all, the rotation range of the actuator and the motion performance of the vehicle with robust controller are analyzed under the condition where saturation is neglected. Then, according to the analysis conclusion, the controller is improved by using linear active disturbance rejection control (LADRC) method, which provides the additional control component to reduce the rotation angle and rotation speed of the actuator. Finally, the simulation proves that the solution could realize the stable motion of vehicle without saturation of actuator.

Keywords: supercavitating vehicle; motion control; actuator saturation; active disturbance rejection control

1. Introduction

A supercavitating vehicle sailing at high speed separates itself from the liquid with a cavity on its surface, which is called hydraulic cavitation. Compared with a traditional full-wet underwater vehicle, a supercavitating vehicle has greatly reduced the frictional resistance caused by the liquid, which leads to a highly increased speed of a supercavitating vehicle. Therefore, supercavitation technology is also known as a revolutionary method to reduce the resistance and increase the cruise speed of a supercavitating vehicle. As the fastest underwater weapon, supercavitating vehicle is studied by many

underwater weapon experts.

For the research of supercavitating vehicles, many scholars have published their research results for modeling, system control and so on, and these results have promoted the development of theoretical and experimental researches for supercavitating vehicles. For example, a four-state and two-degree-of-freedom model in the longitudinal plane was proposed by Dzielski and Kurdila [1] proposes, which retains almost all state information of a supercavitating vehicle, and features simple structure and easy analysis. A six-degree-of-freedom mathematical model for a supercavitating vehicle was formally put forward in a paper [2] which retains more state information of the HSSV and is suitable for scenarios where more state information is analyzed. Semennenko and Arndt, REA et al. [3,4] conducted a lot of hydrodynamic researches on cavities, HSSVs, model for HSSVs and carried out cavity shape calculations, related water tunnel tests, etc. These tasks provided a theoretical basis for the control research of a supercavitating vehicle. Sanabria et al. [5] conducted a series of studies on experimental models of supercavitating vehicles in the water tunnel, and obtained the force coefficients of cavitators in motion. In these studies [6], test platforms and schemes for testing mathematical model and control algorithm are presented. On the other hand, in recent years, hydrodynamic mathematical models of HSSVs have been continuously optimized or improved thanks to the improvement of experimental conditions [7,8]. Due to the fact that a supercavitating vehicle is wrapped by a cavity, the forces on a supercavitating vehicle are affected by a cavity, and the control of a supercavitating vehicle is also more difficult than a full-wet underwater vehicle. In view of this, many scholars have also proposed their own control schemes. Kirschner and Zhang et al. [9] used accurate cavitator, fin models and a linear quadratic controller (LQR) for solutions to horizontal and straight motion as well a tilt-turn control of a supercavitating vehicle. The switching controller selected different LQRs to realize the switching control of a non-linear supercavitating vehicle model with planning force and a linear supercavitating vehicle model without planning force [10]. Another switching control law was also advanced, which is applied to feedback linearization models with or without planning force [11]. As per Vanek et al., a supercavitating vehicle was controlled by a dual-loop controller. The inner loop controller was designed based on a dynamic inversion technique and used to control the stability performance of the HSSV. While the outer loop controller was designed by pole place or receding horizon control (RHC), which is available for the control of the dynamic performance of a supercavitating vehicle. A stable and controllable feasible scheme was put forward based on linear parameter varying controller (LPV) for an uncertainty model of the HSSV, typically the LPV-H inf scheme [12]. Robust control, as a classical control method, is suitable for nonlinear systems, uncertain parameter systems, or time-delay uncertain systems [13−15]. Although the applicable range of the robust controller is rather wide, the synthesis of robust controller remains very complicated and cumbersome. Therefore, the sliding mode controller is widely used as an alternative to simplify controller design. Although the sliding mode controller has been simplified for its comprehensive design, the sliding mode control still has good robustness and ability to reject model uncertainties and external disturbance [16−18]. Qiang [19] Considers the problem of the actuator saturation, proposed a new output feedback control law that locally stabilizes the closed-loop system to enlarge the domain of attraction subject to actuator saturation. But, this article does not consider the effect of the saturation of the angular velocity of the actuator on the motion stability.

It can be seen from the above literature that a large number of researchers focus on the processing of the model and quote the corresponding control algorithm to achieve stable motion control. However, due to the characteristics of supercavitating vehicle, the model itself can not be accurately described

in most cases, which makes it difficult for the traditional control scheme to realize the requirements of stable motion control independently.

Therefore, in order to find the control methods that can adapt to the characteristics of supercavitating vehicle, this paper analyzes the control methods that have been widely used in other engineering fields: in reference [20] DERs are integrated with IEEE 33 bus system using fuzzy logic controller and game theory for two different cases with unity and 0.9 power factor. In reference [21] discusses the control system design of generator rotor speed that is tolerant of faulty sensors and actuators，the sensor and actuator faults estimates are obtained by an extended state observer which realizes a new state from a filtered signal of the measurement, then the sensor fault estimate is submitted to a compensation mechanism in order to correct measurement value while the actuator fault estimate is used to reconfigure control signal value in order to correct control signal. In reference [22] discusses on adaptive protection of microgrids, including a wide range of applicability variants, their strengths, and drawbacks and explores the state-of-the-art researches that utilize computational intelligence to achieve adaptive protection.

In conclusion, fuzzy control [20], fault-tolerant control [21], adaptive control [22], these three algorithms have low dependence on the model and have good adaptability to the supercavitating vehicle model. By comparison，among these control schemes, adaptive control has the advantages of being independent of the model itself and compensating control only according to the output, which is very suitable for the supercavitating vehicle model. Therefore, this paper decides to use adaptive control to study the stable motion control of supercavitating vehicle.

In this paper, the state feedback controller with strong robustness is designed for the supercavitating vehicle using robust pole assignment algorithm [23], which can maintain the stability of the vehicle even if the system parameters change in a limited range. However, it may cause the limit cycle behavior by which the linear controller controls the nonlinear system, therefore, the circular criterion is used to study whether there will be a limit cycle behavior near the equilibrium point. In addition, because this linear robust controller may also lead to actuator saturation, this paper uses LADRC technology to design the automobile outer loop controller, which provides an additional control component for the automobile to reduce the rotation amplitude and speed of the actuator.

The remaining sections are arranged as follows: in Section 2, the longitudinal model of the supercavitating vehicle and in Section 3, a state feedback controller for vehicle was designed by robust pole assignment. The ability of the linear controller to control the nonlinear system was evaluated according to the circle criterion, and it was judged whether the limit cycle could form near the equilibrium point. From the fluid mechanics point of view, the mechanism of cavity instability induced by the actuator was described in definitely. In Section 4, the linear active disturbance rejection controller (LADRC) is introduced as the outer-loop controller which could reduce the rotation angle and the speed of the actuator. After that, the analysis is done for state boundaries and tracking performance of the control system. In Section 5, simulation verifies that the LADRC could realize the stable motion of vehicle without actuator saturation.

2. Longitudinal model of the HSSV

The schematic diagram of an HSSV traveling in water and maintaining a stable cavity is shown in Figure 1.

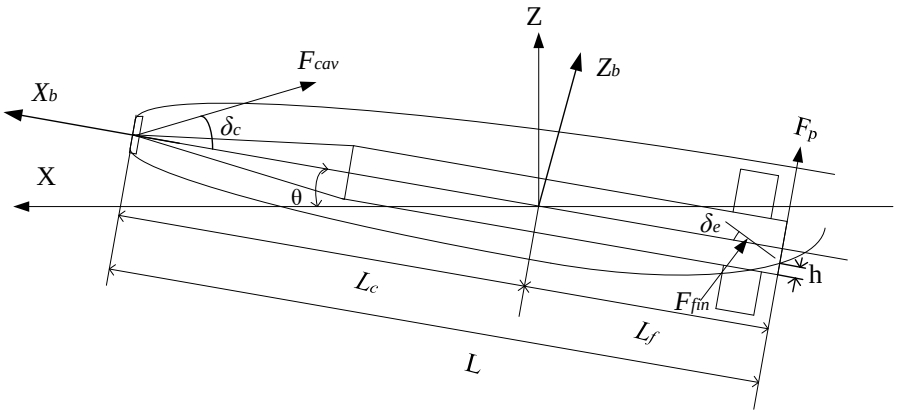

Figure 1. The shape and force diagram of HSSV.

In the longitudinal plane, the body coordinate $X_bY_bZ_b$ is selected for establishing the Longitudinal model of the HSSV. In Figure 1, the main forces on the HSSV include F_{cav} originated from the cavitator, F_{fin} rested on fins, its own gravity F_g, and the possible planning force F_p. δ_c is the deflection angle of the cavitator, which is relative to the body centerline, and the counterclockwise direction is defined as the positive direction. δ_e is the deflection angle of the fin against the body centerline, and the counterclockwise direction is defined as the positive direction. The immersion depth at the fin of the HSSV is h. The total length of the HSSV is L. The distance from the center of gravity to the center of the cavitator is x_g, and the distance from the center of gravity to the fin of the HSSV is x_f.

2.1. Motion analysis for the HSSV

Referring to the model presented by Dzielski and Kurdila [1], the mass of the vehicle M, the distance x_g, and the moment of inertia I are expressed as:

$$\begin{aligned} M &= \frac{7}{9} m\rho\pi R^2 L \\ I &= \frac{11}{60} m\rho\pi R^4 L + \frac{133}{405} m\rho\pi R^2 L^3 \\ x_g &= \frac{17}{28} L \end{aligned} \tag{1}$$

m is the density ratio, ρ is the density of water, and R is the HSSV radius.

In the longitudinal plane, the motion Eqs (2)−(4) of the vehicle can be expressed by several parameters, such as the speed V_x on the X_b axis and V_y on the Z_b axis, the position x on the X_b axis and z on the Z_b axis, the pitch angle θ and the pitch angle speed ω.

$$\dot{x} = V_x \cos\theta - V_y \sin\theta \tag{2}$$

$$\dot{z} = V_x \sin\theta + V_y \cos\theta \tag{3}$$

$$\dot{\theta} = \omega \tag{4}$$

2.2. Dynamic model of supercavitating vehicle

According to the momentum theorem and the momentum moment theorem, the dynamic model is presented as follows:

$$\begin{aligned} F_b &= M(\dot{V} + \omega \times V) \\ M_b &= \dot{H} + \omega \times H \end{aligned} \tag{5}$$

The symbol H denotes the moment of momentum. In addition, the symbol ω denotes the angular speed of the body, and the symbol V is the total velocity of the body. The symbol F_b denotes the total force on the Z_b axis, which includes the force acting on the cavitator F_L on the Z_b axis, the gravity F_g, the lift acting on the fin F_{fin}, the thrust component F_{Tz} on the Z_b axis, and planning force F_p.

$$F_b = F_L + F_{fin} + F_g + F_P + F_{Tz} \tag{6}$$

The symbol M_b denotes the total moment on the Z_b axis, which includes the lift moment on the cavitator M_L, the lift moment on the fin M_{fin}, the moment of gravity M_g, the moment of thrust M_{Tz}, and the moment of planning force M_p.

$$M_b = M_L + M_g + M_{fin} + M_{Tz} + M_p \tag{7}$$

The force acting on the cavitator F_{cav} is expressed as

$$F_{cav} = C_{cav}\delta_c \tag{8}$$

where $C_{cav} = (1/2)\rho V^2 \pi R_n^2 C_{x0}(1+\sigma)$, and it represents the cavitator efficiency. The relationship between the deflection angle of the cavitator δ_c and the attack angle of the cavitator α_c is expressed as:

$$\alpha_c = \tan^{-1}\left(\frac{V_y}{V} + \frac{qx_g}{V}\right) + \delta_c \tag{9}$$

F_{cav} can be decomposed into Lift F_L and Drag F_D acting on the cavitator, which are expressed as

$$F_L = (1/2)\rho V^2 \left(\pi R_n^2\right) C_{x0}(1+\sigma)\cos\alpha_c \sin\alpha_c \tag{10}$$

$$F_D = -(1/2)\rho V^2 \left(\pi R_n^2\right) C_{x0}(1+\sigma)\cos^2\alpha_c \tag{11}$$

The lift moment on the cavitator is

$$M_L = F_L x_g \tag{12}$$

The lift and moment on the fin are denoted separately as

$$\begin{aligned} F_{fin} &= n(1/2)\rho V^2 \left(\pi R_n^2\right) C_{x0}(1+\sigma)\cos\alpha_f \sin\alpha_f \\ M_{fin} &= F_{fin} x_f \end{aligned} \tag{13}$$

where α_f is the attack angle of the fin, and the relationship between α_f and the deflection angle δ_f is as follows

$$\alpha_f = \tan^{-1}\left(\frac{V_y}{V} + \frac{qx_f}{V}\right) + \delta_f \tag{14}$$

The resistance originated from the fin can be expressed as

$$F_{fin\_D} = -n(1/2)\rho V^2\left(\pi R_n^2\right)C_{x0}\left(1+\sigma\right)\cos^2\alpha_f \tag{15}$$

The gravity of the vehicle $F_g = Mg\cos\theta$. Because the origin of the coordinates $X_bY_bZ_b$ coincides with the gravity center of the vehicle, the gravity moment M_g equals to 0.

Due to the gravity or the disturbance to the speed of the HSSV, the fin of the HSSV is in contact with the cavity wall. Due to the fact that the difference between the speed of the HSSV and that of the speed of the surrounding water flow is huge, when the HSSV collides with the cavity wall, it will occur in a short time that a large recovering force is generated to bounce the HSSV back into the cavity, and this recovering force is called the planning force. F_p and M_p respectively represent the component of the planning force on the Z_b axis and the corresponding moment, which are specifically expressed as Dzielski and Kurdila [1]:

$$\begin{cases} F_p = -\pi\rho R^2V^2(1-\dfrac{R_c-R}{hR-R_c+R})^2(\dfrac{1+h}{1+2h})\alpha_p \\ M_p = F_pL_f \end{cases}$$

$$\alpha_p = \begin{cases} \dfrac{V_y-\dot{R}_c}{V} & \dfrac{V_y}{V} > 0 \\ \dfrac{V_y+\dot{R}_c}{V} & otherwise \end{cases} \qquad h = \begin{cases} \dfrac{L|V_y|}{RV} - \dfrac{R_c-R}{R} & otherwise \\ 0 & \dfrac{R_c-R}{R} > \dfrac{L|V_y|}{RV} \end{cases} \tag{16}$$

$$k_1 = \frac{L}{R}(\frac{1.92}{\sigma}-3)^{-1}-1,\quad k_2 = (1-(1-\frac{4.5\sigma}{1+\sigma})k_1^{\frac{40}{17}})^{\frac{1}{2}}$$

$$R_c = R_n(0.82\frac{1+\sigma}{\sigma})^{\frac{1}{2}}k_2,\quad \dot{R}_c = -\frac{20}{17}(0.82\frac{1+\sigma}{\sigma})^{\frac{1}{2}}V\frac{(1-\frac{4.5\sigma}{1+\sigma}k_1^{\frac{23}{17}})}{k_2(\frac{1.92}{\sigma}-3)}$$

The thrust component of the vehicle on the Z_b axis and the thrust component on the X_b axis are expressed respectively

$$F_{Tz} = 0 \tag{17}$$

$$F_{Tx} = F_T \tag{18}$$

Because the thrust acts on the center of gravity, the moment of the thrust is expressed as follows:

$$M_T = 0 \tag{19}$$

Assuming that the vehicle is in constant motion along the X_b axis, the dynamic equation on the X_b axis is expressed as follows:

$$M\dot{V}_x = F_D + F_T + F_{fin\_D} = 0 \tag{20}$$

Therefore, the thrust of the vehicle can be expressed as:

$$F_T = \left(-1-n\right)C_{cav} \tag{21}$$

The dynamic model of vehicle can be expressed as:

$$\begin{aligned} M\dot{V}_y &= F_L + F_{fin} + F_g + F_p \\ I\dot{\omega}_y &= F_L x_g + F_{fin} x_f + F_p x_f \end{aligned} \tag{22}$$

2.3. Longitudinal model of supercavitating vehicle

Combining motion Eq (3) with angular relation Eq (4), let $x_1 = z,\ x_2 = V_y,\ x_3 = \omega,\ x_4 = \theta$ and give the final longitudinal model shown in Eq (23), the technical parameters of this model are the same as those Dzielski and Kurdila [1] shown in Table 1.

$$\begin{cases} \dot{x}_1 = x_2 - Vx_4 \\ \dot{x}_2 = (\dfrac{n-1}{MV}C_{cav})x_2 + (\dfrac{x_g - nx_f}{MV}C_{cav})x_3 \\ -\dfrac{C_{cav}}{M}\delta_c + \dfrac{nC_{cav}}{M}\delta_f - g \\ +\dfrac{\pi\rho R^2V^2}{M}(1-\dfrac{R_c-R}{hR-R_c+R})^2(\dfrac{1+h}{1+2h})\alpha_p \\ \dot{x}_3 = (\dfrac{nx_f - x_g}{IV}C_{cav})x_2 + (\dfrac{x_g^2 - nx_f^2}{IV}C_{cav})x_3 \\ -\dfrac{C_{cav}x_g}{I}\delta_c + \dfrac{nC_{cav}x_f}{I}\delta_f \\ +\dfrac{\pi\rho R^2V^2x_f}{I}(1-\dfrac{R_c-R}{hR-R_c+R})^2(\dfrac{1+h}{1+2h})\alpha_p \\ \dot{x}_4 = x_3 \end{cases} \tag{23}$$

Table 1. Parameter of the HSSV.

parameter	description	value
g	gravitational acceleration	9.81 m/s^2
m	density ratio	2
M	mass	22 kg
L	length	1.8 m
n	rudder efficiency	0.5
R_n	radius of cavitator	0.0191 m
R	HSSV radius	0.0508 m
V	total speed	75 m/s
σ	cavitation number	0.03

3. Controller design and stability analysis

3.1. Controller design of robust pole assignment

Due to the existence of inevitable modeling error, this section selects the robust pole assignment algorithm to design the controller for vehicle, though eigenvalues of a matrix are sensitive to design the controller for vehicle [23].

Though eigenvalues of a matrix are sensitive to perturbation of elements in the matrix, eigenvalues of the normal matrix are less sensitive to this perturbation.

Theorem 3.1: The reference model based on Eq (23) with parameters changes is expressed as follows:

$$\begin{cases} \dot{x} = (A + \Delta A)x + (B + \Delta B)u \\ y = (C + \Delta C)x \\ x(0) = x_0 \end{cases} \tag{24}$$

The state feedback controller Eq (25) is added to Eq (24).

$$u = Kx + v \tag{25}$$

The closed-loop system is expressed as:

$$\dot{x} = (A + BK)x + (\Delta A + \Delta BK)x + (B_o + \Delta B)v \tag{26}$$

If the system is controllable, the desired state feedback matrix K satisfies.

$$(A + BK)X = X\Lambda \tag{27}$$

where $\Lambda = diag(\lambda_1, \cdots, \lambda_n)$ is the system eigenvalues matrix, the condition number of Matrix X needs to be as small as possible, which makes the desired closed-loop poles robust.

The steps of robust pole assignment are as follows [19]:

Step1: By means of the use of QR decomposition method, factorize of matrix B and $\left[U_1^T(A - \lambda_i I)\right]^T$:

$$B = [U_0 \quad U_1]\begin{bmatrix} Z \\ 0 \end{bmatrix}, \left[U_1^T(A - \lambda_i I)\right]^T = \begin{bmatrix} \hat{S}_i & S_i \end{bmatrix}\begin{bmatrix} R_i \\ 0 \end{bmatrix} \tag{28}$$

where S_i is a group base of the Nuclear Space $Ker[U_1^T(A - \lambda_i I)]^T$.

$$X_i = S_i\zeta_i \tag{29}$$

where ζ_i is p dimensional column vector, and p is the number of columns of Matrixes B.

Step2: Select a vector ζ_i available to have Matrix X satisfy Eq (27) and make condition number $k_F(X(\zeta)) = \|X\|_F \bullet \|X^{-1}\|_F$ of Matrix X as small as possible.

Step3: Search direction d_k is obtained using quasi-Newton method and step size in search a_k is obtained under inexact line searches(Armijo Goldstein rule), therefore, new coordinate vector is $\zeta_{k+1} = \zeta_k + a_k d_k$.

Step4: Gradient and norm of Matrix X and condition number $k_F(X(\zeta))$ on point ζ_{k+1} are

calculated; return to Step 3 if the norm is more than system error, otherwise continue with the next step.

Feedback matrix K is given by

$$K = Z^{-1}U_o^T(X\Lambda X^{-1} - \Lambda) \tag{30}$$

Theorem 3.2: (Bauer-Fike rule Theorem): if $E \in R^{n\times n}$, $\mu \in C$ is characteristic value of matrix (A+BK+E), in that case, the characteristic value of matrix (A+BF) will meet the demand in Eq (31).

$$\left|\lambda - \mu\right| \le K_F(X)\left\|E\right\|_2 \tag{31}$$

If the condition number $k_F(X(\zeta))$ is limited, the change rate of its characteristic value will not exceed $k_F(X(\zeta))$ times the change rate of $\|E\|_2$. When $\|E\|_2$ approaches to 0, the change rate of the pole can be controlled. However, once $k_F(X(\zeta)) \equiv \infty$, there must be an infinite sensitivity of the eigenvalue λ to the change of the matrix. At this time, the model needs to be redesigned or other hidden conditions need to be considered [24].

In order to reflect the situation of exceeding the actual working range of the actuator in the theoretical simulation of supercavitating vehicle motion control, the following example is given here. To realize fixed-depth constant motion of the supercavitating vehicle in the longitudinal plane，the expected poles are selected as −5, −15, −58, −178. According to Theorem 3.1 and Theorem 3.2, the minimum condition number for vehicle model which has a system error of 10% was searched. By conducting 126 searches, the minimum condition number is obtained as $k_F(X(\zeta)) = 6.2895 \times 10^5$, therefore, the feedback Matrix K is as follows.

$$K = \begin{bmatrix} 100.1615 & -1.2001 & -3.2425 & -50.02 \\ -3.4707 & 0.4148 & 1.0375 & 62.8821 \end{bmatrix} \tag{32}$$

In this section, the mature robust pole design method is used in the controller design, and the obtained controller will be used as the basis for analyzing the actuator saturation phenomenon in the motion control of supercavitating vehicle, but this controller design part is not the point of this paper.

3.2. Analysis of simulation results

The Figures 2−4 show the state of motion of the supercaviting vehicle after robust pole assignment, the planning force at the fin of the vehicle, and the immersion depth as well as the rotation angle and rotation speed of the cavitator and the fin.

Under the joint control of the cavitation and the fin, the supercavitating vehicle in Figure 2 finally showed the state of fixed-depth constant motion.

As shown in Figure 3, during the movement of the vehicle, the fin of the vehicle is in direct contact with the cavity wall and glides along the cavity wall to form the planning force; while the fin will support the fin of the vehicle, and the vehicle motion state does not suffer from a limit cycle behavior. However, as shown in Figure 4, this state of motion is with a problem that the cavitator and the fin turn at too high speed which cannot be achieved by the actual motor, and too high turning speed will also cause damage to the stable motion state of the vehicle.

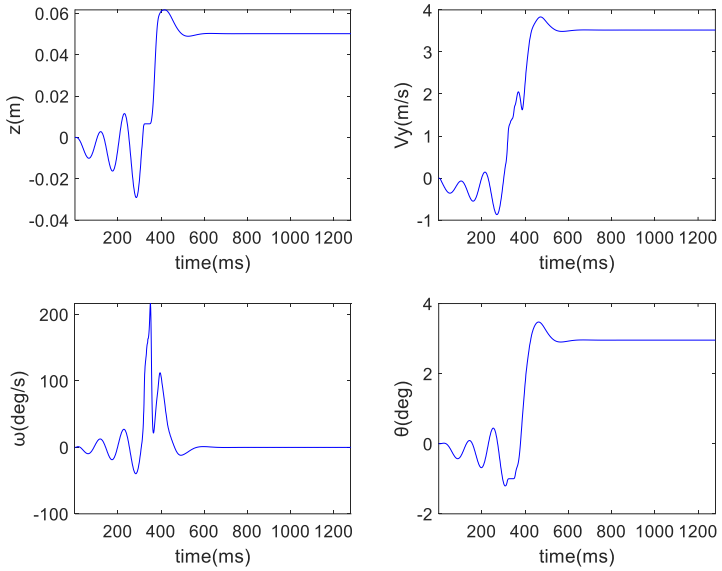

Figure 2. The motion states of HSSV.

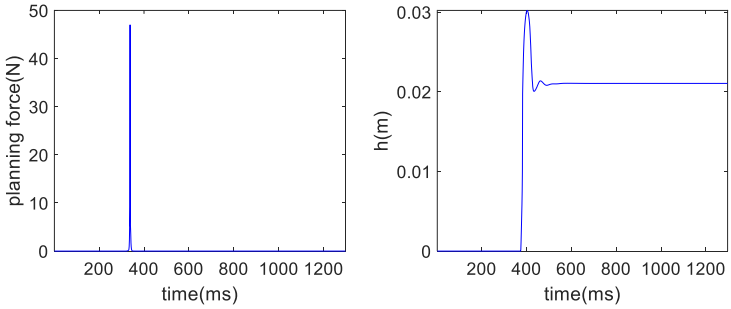

Figure 3. The planning force and immersion depth of HSSV.

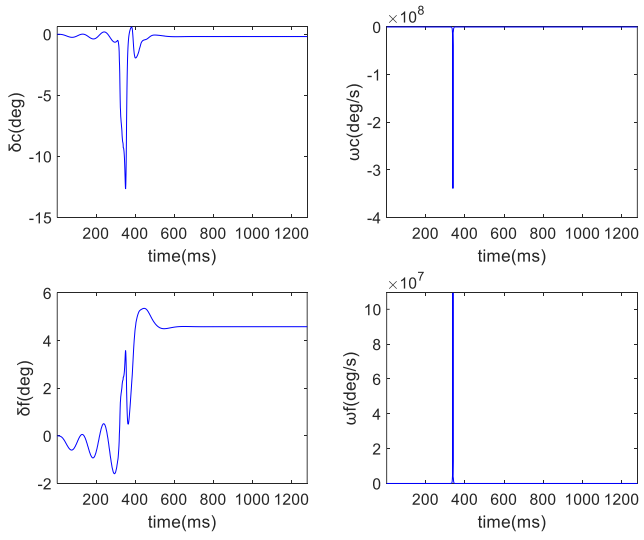

Figure 4. The degree and rotate velocity of actuator of HSSV.

3.3. Evaluation of control ability of linear feedback controller

Although the simulation results obtained in Section 3.2 show that the system runs stably without limit cycle behavior in 0~2 s, it does not mean that the system can maintain such a state in the future.

Moreover, the linear feedback control method is prone to cause limit cycle behavior at the equilibrium point [1], which destroys the stability of the system.

In this section, the circle criterion will be used to evaluate the control ability of the above linear feedback controller for nonlinear systems, and predict whether it is possible to produce limit cycle behavior.

As shown in Eq (33), following Lure-form systems exist (Figure 5), in which the linear portion is $G(s)=C(sI-A)^{-1}B$, symbol s refers to Laplacian operator, and $\psi(\cdot)$ referring to the nonlinear portion satisfies the sector condition (34).

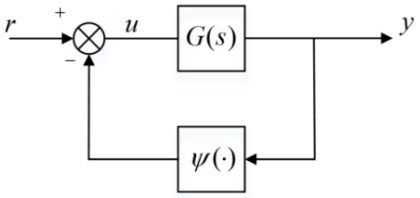

Figure 5. Lure form system for application of circle criterion.

$$\begin{cases} \dot{\boldsymbol{x}} = \boldsymbol{A}\boldsymbol{x} + \boldsymbol{B}\boldsymbol{u} \\ \boldsymbol{y} = \boldsymbol{C}\boldsymbol{x} + \boldsymbol{D}\boldsymbol{u} \\ \boldsymbol{u} = -\psi(t, \boldsymbol{y}) \end{cases} \tag{33}$$

$$\alpha y^2 \le y\psi(y) \le \beta y^2, \quad \forall y \in [a,b] \tag{34}$$

Theorem 3.3: (circle criterion)**:**

When Nyquist plot $G(j\omega)$ of the single input and single output system is on the right side of the vertical line $\mathrm{Re}[s] = -1/\beta$, and the system meets the requirement of $0 = \alpha < \beta$, then the system is absolutely stable ($-a = b = \infty$). However, when the sector condition (34) is only established in a finite interval $[a,b]$, the region of attraction (ROA) of the equilibrium point can be estimated with the Lyapu function.

The evaluation values of the region of attraction are as follows:

$$\Omega = \{x \in R^4 \,|\, V(x) = x^T P x \le c_3\} \tag{35}$$

where $c_3 = \min V(x)$, and matrix P and scalar ε satisfy the following Riccati equation.

$$P\left[\frac{\varepsilon I}{2} + A\right] + \left[\frac{\varepsilon I}{2} + A^T\right]P + (KC^T - PB)\frac{1}{2}(KC - B^T P) = 0 \tag{36}$$

The positive real scalar ε must satisfy the requirements that $1 + \beta G(s - 0.5\varepsilon)$ and $(\varepsilon/2)I + A$ are to be Hurwitz [12].

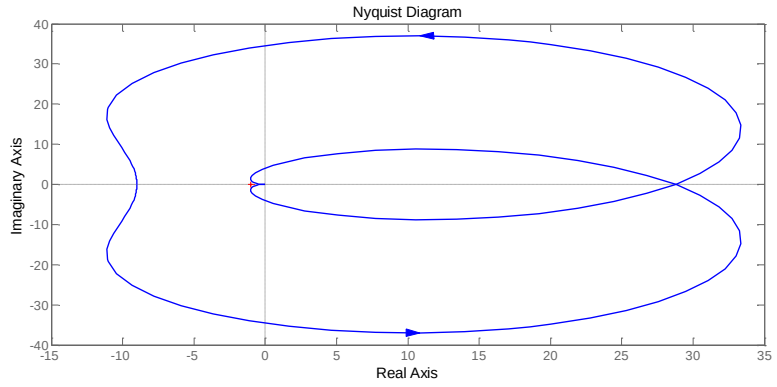

Figure 6. Nyquist diagram of G(s).

The nonlinear component is globally located in the sector condition [0, β = 85]. It can be seen easily that the nyquist curve of the transfer function G(s) from δ_c to V_y in Figure 6 does not meet the requirements of sufficient conditions for global absolute stability.

However, controller (32) can make the system locally stable in the finite interval y = $V_y \in [-3.5, 3.5]$ and under the sector condition [0, 76] (ε = 0.02). In addition, the evaluation value of the region of attraction (the equilibrium point x is [0, 3.5, 0,3])

$$\Omega = \{x \in R^4 \mid V(x) = x^T P x \le 21.3611\} \tag{37}$$

$$P = \begin{bmatrix} 0 & 0 & 0 & 0 \\ 0 & 1.7987 & -0.5388 & -0.0082 \\ 0 & -0.5388 & 0.2496 & 0.0038 \\ 0 & -0.0082 & 0.0038 & 0.0114 \end{bmatrix} \tag{38}$$

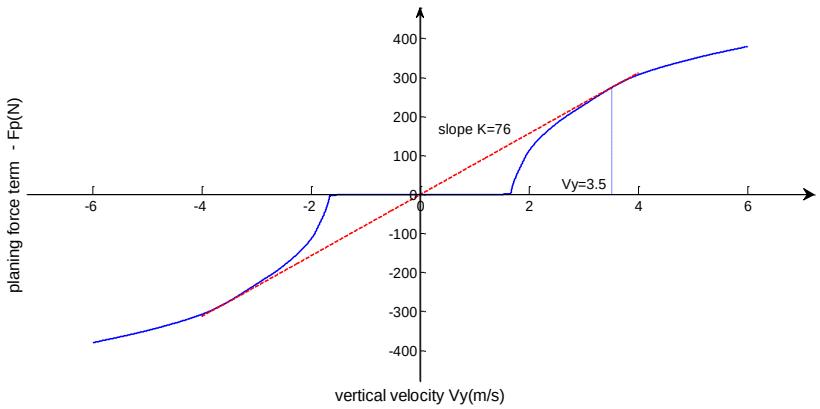

Figure 7. ROA estimation using circle criterion.

From the above results, it can be concluded that the region Ω is within the set $\{|V_y| \le 3.5\}$ and the system is absolutely stable in the limited region. The linear controller designed in Section 3.1 is effective for the control of nonlinear systems, and the closed-loop system is available to resist large-scale planning force interference in the region of attraction. During the motion, the fin of the vehicle

is supported by the fin, and. in the time domain simulation (Figure 2), the system does not form limit cycle behavior. Therefore, in the vicinity of the equilibrium point, the system will remain stable and out of limit cycle behavior. However, this control method will bring about the phenomenon of actuator saturation (Figure 3), therefore, this problem will be solved in Section 4 with a linear active disturbance rejection controller.

3.4. Hydrodynamic causes of cavity instability induced by actuators

From the perspective of hydrodynamics, this section attempts to figure out the reasons for the instability of the cavity induced by the movement of actuators when actuators exceed the angular range and the angular rate range.

When the vehicle is sailing at high speed in the water, the pressure of the liquid behind the tip of the cavitator is lower than the vapor pressure, and shedding will begin to occur [25]. Shedding is the result of interaction between the bubble and the boundary layer of fluid in front of the bubble. Besides, these small bubbles converge at the fin of the vehicle to form a closed cavity to enclose the vehicle [26,27]. The cavitator has direct impacts on the internal pressure and flow rate of bubbles by changing the starting point of the shedding, thereby adjusting the position and shape of the cavity. The HSSV is based on this principle to adjust the movement attitude of the vehicle and the cavity, while ensuring that the cavity is not broken.

However, the movement of actuators will cause disturbances and further cause the cavity to fall off or even collapse of the cavity [28,29]. The reason is that when the cavitator turns at high speed, the delay effect of tip leakage vortex cavitation is strengthened and the maximum volume of the cavity is reduced [30]. When a new disturbance is triggered by the cavitator, the pressure of the cavity wall changes again, while the cavity will no longer be maintained in the optimal state. Since the change of cavity shape is a delayed process which is superimposed with the previous change of cavity shape, the current change will be more intensified than the previous one, even if it may induce cavity instability. In view of the size of the cavity, if the angle of attack is too large, it will be easy to cause the rear of the vehicle to scour the cavity and destroy the stability of the cavity. On the other hand, continuous disturbance caused by a cavitator would lead to a huge impact on the boundary leakage mechanism of the cavity. In the case that the cavitator swings relatively fast, a strong momentum exchange will occur at the water-vapor interface. When the liquid velocity is greater than that of the water-vapor mixing zone, the liquid will bring bubbles out of the cavity boundary and cause gas leakage. When bubbles velocity inside the cavity boundary is greater than that in the liquid, the liquid will be entrained toward the interior of the cavity under the influence of gravity. As the result, a fierce jet is formed to destroy the stability of the cavity, as shown in Figure 8. Based on the instability of these two causes, a vortex will be generated near the cavity boundary or on the cavity body. Sometimes this vortex is critically stable, but it is prone to be unstable due to external disturbance. Unfortunately, it is a potential reason for the instability of the cavity, this phenomenon should be avoided.

The effect of turning the fin is similar to that of the cavitator. At the same time, the hydrodynamic at the fin of the cavity is very complicated. Besides, the turbulence and vortices generated by fins are more harmful to the stability of the cavity [31]. Therefore, in order to stabilize the cavity, it is truly necessary to limit the angular range and angular rate range of fins.

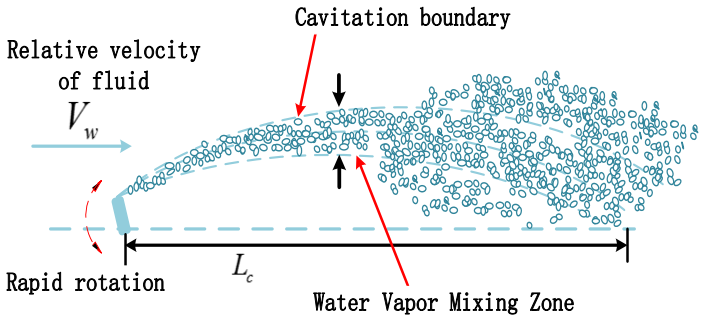

Figure 8. Instability caused by rapid rotation of cavitator.

4. Design of anti saturation controller

4.1. Concept for LADRC

The core idea of LADRC theory is to use a linear expansion state observer (LESO) to estimate the unknown generalized disturbance and suppress the disturbance.

Assume the following linear system:

$$a_n y^{(n)}(t) + a_{n-1} y^{(n-1)}(t) + \cdots + a_1 \dot{y}(t) + a_0 y(t) = b_m u^{(m)}(t) + \cdots b_1 \dot{u}(t) + b_0 u(t) + c_h d^{(h)}(t) + \cdots c_1 \dot{d}(t) + c_0 d(t) \quad (39)$$

where *y(t)*, *u(t)* and *d(t)* are the output, input and disturbance of the system respectively.

Active disturbance rejection control does not need to be based on the accurate model of the controlled object and the disturbance, however, the relative order $p = n\text{-}m$ and gain $b = b_m/a_n$ must be specified.

It is generally assumed that the controlled system includes the following model:

$$y^{(p)}(t) = bu(t) + f(y(t), u(t), d(t)) \quad (40)$$

where *y(t)*, *u(t)* and *d(t)* are the output, input and disturbance of the system respectively, in addition, *p* and *b* are two known parameters of the controlled system, and *f(y, u, d)* is the combination of unknown dynamics of the system and external disturbance, which is assumed to be unknown in the design of the LADRC and called as generalized perturbation.

Set the status of the system as:

$$z_1 = y, z_2 = \dot{y}, \ldots, z_p = y^{(p-1)}, z_{p+1} = f(y, u, d) \quad (41)$$

Let *f(y, u, d)* be differentiable and $\dot{f}(y,u,d) = h(t)$, then the systemic model Eq (23) can be written as:

$$\begin{cases} \dot{z} = A_o z + B_o u + E_o h \\ y = C_o z \end{cases} \quad (42)$$

where $z = [z_1 \quad z_2 \quad \cdots \quad z_p \quad z_{p+1}]^T$

$$A_o=\begin{bmatrix}0&1&0&\cdots&0\\0&0&1&\cdots&0\\\vdots&\vdots&\vdots&\ddots&\vdots\\0&0&0&0&1\\0&0&0&0&0\end{bmatrix}_{(p+1)\times(p+1)}\quad B_o=\begin{bmatrix}0\\0\\\vdots\\b\\0\end{bmatrix}_{(p+1)\times 1}\quad E_o=\begin{bmatrix}0\\0\\\vdots\\0\\1\end{bmatrix}_{(p+1)\times 1}\quad C_o=\begin{bmatrix}1&0&0&\cdots&0\end{bmatrix}_{1\times(p+1)}$$

Design a full-order Luenberger observer for this system. In the case that the observer is not only used to observe the systemic output and its each derivative, but also observe generalized disturbance, this observer is also called a linear expansion state observer (LESO).

$$\begin{cases}\dot{\hat{z}}=A_o\hat{z}+B_ou+L_o(y-\hat{y})\\\hat{y}=C_o\hat{z}\end{cases}\tag{43}$$

where L_o is the linear observer gain: $L_o=\begin{bmatrix}\beta_1&\beta_2&\cdots&\beta_p&\beta_{p+1}\end{bmatrix}^T$

The poles of the observer are arranged at $-\omega_o$, the characteristic equation of $A_O-L_OC_O$ is: $\left|SI-(A_O-L_OC_O)\right|=s^{p+1}+\beta_1 s^p+\cdots+\beta_{p+1}=(s+\omega_o)^{p+1}$ and where $\binom{p+1}{i}$ is the combination coefficient, and ω_o is the bandwidth of the observer. The gain of observer L_o is independently decided by the parameter ω_o.

Use the following control law:

$$u(t)=\frac{-\hat{z}_{p+1}(t)+u_o(t)}{b}\tag{44}$$

where $u_o(t)$ is the item to be determined, then, model Eq (40) becomes:

$$y^{(p)}(t)=u_o(t)-\hat{z}_{p+1}(t)+f(y(t),u(t),d(t))\tag{45}$$

When LESO is designed appropriately, $\hat{z}_{p+1}\approx f(y(t),u(t),d(t))$ and the system becomes a p-order integral system, that is:

$$y^{(p)}(t)\approx u_o(t)\tag{46}$$

This system may adopt the following state feedback control law:

$$u_o(t)=k_1(r(t)-\hat{z}(t))+k_2(\dot{r}(t)-\dot{\hat{z}}(t))+\cdots+k_p(r^{(p-1)}(t)-\hat{z}^{(p-1)}(t))\tag{47}$$

where $r(t)$ represents the reference signal. Due to the fact that $\hat{z}_1(t),\cdots,\hat{z}_p(t)$ approach $y(t),\cdots,y^{(p-1)}(t)$ respectively, the final control law can be expressed as:

$$u(t)=\frac{k_1(r(t)-\hat{z}_1(t))+\cdots+k_p(r^{(p-1)}(t)-\hat{z}_p(t))}{b}-\frac{\hat{z}_{p+1}(t)}{b}=K_o(\hat{r}(t)-\hat{z}(t))\tag{48}$$

where $\hat{r}(t)$ is the generalized reference signal, which is a vector consisting of the reference signal and each of its order derivative.

$$\hat{r}(t)=\begin{bmatrix}r(t)&\dot{r}(t)&\cdots&r^{(p-1)}(t)&0\end{bmatrix}^T\tag{49}$$

The state feedback gain K_o is defined as:

$$K_o = \begin{bmatrix} k_1 & k_2 & \cdots & k_p & 1 \end{bmatrix} \frac{1}{b} \tag{50}$$

The poles of the state feedback controller are arranged at $-\omega_c$ and the characteristic equation of $A_O - B_O K_O$ is: $\left|SI - (A_O - B_O K_O)\right| = s(s^p + k_n s^{p-1} + \cdots + k_1) = s(s + \omega_c)^p$

where $k_i = \begin{pmatrix} p \\ i-1 \end{pmatrix} \omega_c^{n-i+1}, i = 1, \cdots, p$; with $n = p$ and $\begin{pmatrix} p \\ i-1 \end{pmatrix}$ is the combination coefficient.

The gain of feedback controller K_o is independently decided by ω_c.

The structure of the LADRC designed for the HSSV is shown in Figure 9.

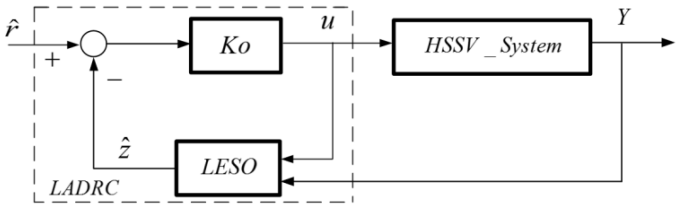

Figure 9. structure of HSSV'S LADRC.

In Figure 9, Y refers to the output of HSSV system and u is the extra control variable provided by the cavitator for the supercavitating vehicle. When designing a linear active disturbance rejection controller for the cavitator, Y are chosen as 3 times of the partial control variable in formula Eq (32) $Y = \mathrm{y} = 300.6x_1 - 3.6x_2 - 9.6x_3 - 150x_4$.

The linear active disturbance rejection controller (LADRC) has the following state space implementation:

$$\begin{cases} u = K_o(\hat{r} - \hat{z}) \\ \dot{\hat{z}} = (A_o - L_o C_o)\hat{z} + B_o u + L_o Y \end{cases} \tag{51}$$

4.2. Systemic bounded input and bounded output (BIBO) and tracking performance analysis

4.2.1. Systemic BIBO analysis

Let the evaluation error of the full-order Luenberger observer be:

$$e = z_i - \hat{z}_i, i = 1, 2 \cdots, p+1, \quad \dot{e} = A_e e + d \tag{52}$$

where

$$A_e = A - LC = \begin{bmatrix} -\beta_1 & 1 & 0 & \cdots & 0 \\ -\beta_2 & 0 & 1 & \cdots & 0 \\ & & & \cdots & \\ -\beta_p & 0 & 0 & \cdots & 1 \\ -\beta_{p+1} & 0 & 0 & \cdots & 0 \end{bmatrix}, \text{ and } \mathrm{d=E}\,h$$

Lemma 1: if the selected parameter $\beta_1,\cdots,\beta_{p+1}$ in the observer gain L_o make A_e Hurwitz stable, the evaluation error *h* of the Luenberger observer is bounded when any bounded generalized error *h* exists.

It is proved as follows: If A_e is Hurwitz stable, now let $V = e^T Pe$ be a Lyapunov function, where P is the only solution to Lyapunov equation $A_e{}^T P + PA_e = -Q$, and Q is a positive definite matrix. Then:

$$\dot{V} = -e^T Qe + 2d^T Pe = -(e^T Q^{\frac{1}{2}} - d^T PQ^{-\frac{1}{2}})(e^T Q^{\frac{1}{2}} - d^T PQ^{-\frac{1}{2}})^T + (d^T PQ^{-\frac{1}{2}})(d^T PQ^{-\frac{1}{2}})^T \tag{53}$$

If

$$\left\| e^T Q^{\frac{1}{2}} - d^T PQ^{-\frac{1}{2}} \right\|_2 > \left\| d^T PQ^{-\frac{1}{2}} \right\|_2 \tag{54}$$

or

$$\left\| e^T Q^{\frac{1}{2}} \right\|_2 > 2\left\| d^T PQ^{-\frac{1}{2}} \right\|_2 \tag{55}$$

$\dot{V} < 0$ establishes.

Specially $Q = I$, if $\|e\|_2 > 2\|Pd\|_2$, $\dot{V} < 0$ also establishes.

Specially, $Q = I$, if $\|e\|_2 > 2\|Pd\|_2$, $\dot{V} < 0$ also establishes.

This means that evaluation error *e* owns a lower bound, once $\|e\|_2 > 2\|Pd\|_2$ establishes. Therefore, *e* is bounded.

It is worth mentioning that Lemma 1 is also applicable to the following dynamic system:

$$\dot{\xi} = \mathrm{M}\xi + g(\xi) \tag{56}$$

where $\xi \in \Re^n, and \quad \mathrm{M} \in \Re^{n\times n}$. Lemma 2 can be given as follows:

Lemma 2: The necessary condition for bounded ξ in Eq (33) is: if and only if M is Hurwitz stable, and at the same time, $g(\xi)$ is stable and bounded.

By connecting Lemma 1 with Lemma 2, we can get the bounded definition of LADRC:

Definition 1: If the appropriate observer Eq (43) and control law Eq (44) are selected, the closed-loop system becomes a p-order integral system ($y^{(p)}(t) \approx u_o(t)$) which is stable. Then the designed LADRC can make the closed-loop system be BIBO stable by Eqs (43), (44) and (47).

Proof is as follows: According to Lemma 1, the evaluation error e of the observer is bounded. Combining Eqs (40), (44) and (47), the LADRC closed-loop system with the relative order $r = p$ can be expressed as:

$$\dot{Z} = \mathrm{P}Z + \mathrm{N}\begin{bmatrix}\lambda \\ e\end{bmatrix} \tag{57}$$

$$\mathrm{P} = \begin{bmatrix} 0 & 1 & 0 & \cdots & 0 & 0 \\ 0 & 0 & 1 & \cdots & 0 & 0 \\ 0 & 0 & \vdots & \ddots & \vdots & 0 \\ 0 & 0 & 0 & \cdots & 1 & 0 \\ 0 & 0 & 0 & \cdots & 0 & 1 \\ -k_1 & -k_2 & -k_3 & \cdots & -k_{p-1} & -k_p \end{bmatrix}_{p\times p} \quad \mathrm{N} = \begin{bmatrix} 0 & 0 & 0 & 0 & \cdots & 0 & 0 \\ 0 & 0 & 0 & 0 & \cdots & 0 & 0 \\ 0 & 0 & 0 & 0 & \cdots & 0 & 0 \\ 0 & 0 & 0 & 0 & \cdots & 0 & 0 \\ 0 & 0 & 0 & 0 & \cdots & 0 & 0 \\ k_1 & \cdots & k_p & k_1 & \cdots & k_p & 1 \end{bmatrix}_{p\times(2p+1)}$$

where $\mathrm{Z}=\begin{bmatrix} y & \dot{y} & \cdots & y^{(p-1)} \end{bmatrix}^T$, $\lambda=\begin{bmatrix} r & \dot{r} & \cdots & r^{(p-1)} \end{bmatrix}^T$

According to Lemma 2, when λ and e are bounded and P is Hurwitz stable, $\bar{X}$ is bounded.

4.2.2 Systemic tracking performance analysis

In Eq (57) includes:

$$y^{(p)} = k_1(r-y)+\cdots+k_p(r^{(p-1)}-y^{(p-1)})+k_1(z_1-\hat{z}_1)+\cdots+k_p(z_p-\hat{z}_p)+(z_{p+1}-\hat{z}_{p+1}) \tag{58}$$

Definition 2: When r = 0, the output of the system is zero input response, and the output only depends on the system structure. Combining Eqs (46) and (47), there is

$$k_1(z_1-\hat{z}_1)+\cdots+k_p(z_p-\hat{z}_p)+(z_{p+1}-\hat{z}_{p+1})=0 \tag{59}$$

Because the coefficients before each term in Eq (59) are not all 0, the necessary conditions for the accurate state observation of LESO can be obtained, that is,

$$z_i \approx \hat{z}_i \tag{60}$$

The output of the closed-loop supercavity vehicle with LADRC designed in Figure 9 is fed back to LESO which is available to accurately track the output and various derivatives

$$y^{(i-1)} \approx \hat{z}_i, i=1,2\cdots p \tag{61}$$

Definition 3: When $r \neq 0$,the output of the system depends not only on the structure of the system, but also on the external input. In the case that Eq (58) is combined with the necessary conditions for LESO accurate state observation (Eq (60)), Eq (62) is given by

$$y^{(p)}(t) = k_1(r(t)-\hat{z}_1(t))+k_2(\dot{r}(t)-\hat{z}_2(t))+\cdots+k_p(r^{(p-1)}(t)-\hat{z}_p(t)) \tag{62}$$

When Y and each of its derivatives are bounded, if and only if parameter k_i of state feedback gain K are all not 0, the evaluation value of LESO and each of their derivative $\hat{z}_i(t)$ converges to the input of the system and each of its derivatives $r^{(i-1)}(t)$.

Proof is as follows: From Definition 1, we know that Y and each of its derivatives are bounded. According to the convergent nature of the series, when $p\to\infty$ and k_i are all not 0, the p-order derivative of systemic output $y^{(p)}(t)$ is equal to 0. Furthermore, the observations of LESO and their derivatives are bounded. If and only if the evaluation value of LESO and each of their derivatives $\hat{z}_i(t)$ are equal to the input of the system and each of its derivatives $r^{(i-1)}(t)$, the conclusion $\hat{z}_i(t)=r^{(i-1)}(t)$ holds. Proof completes.

5. Simulation and results discussion

5.1. Selection of controller parameters

As mentioned above: LADRC must specify the relative order p = n − m and gain $b=b_m/a_n$ of the controlled object. In this paper, the parameters of LADRC are as follows: the relative order p = 2 and gain b = 10. For the design requirements of LADRC, it is also necessary to determine the parameters of ω_c and ω_0. In this paper, ω_c = 6 and the parameter of the observer gain L_o is also determined, that is, ω_0 = 8.

After selecting the parameters, LADRC is designed for the cavitator when LADRC is not designed for the fin, and it can be expressed as:

$$\begin{bmatrix} \dot{\hat{z}}_1 \\ \dot{\hat{z}}_2 \\ \dot{\hat{z}}_3 \end{bmatrix} = \begin{bmatrix} -24 & 1 & 0 \\ -192 & 0 & 1 \\ -512 & 0 & 0 \end{bmatrix} \begin{bmatrix} \hat{z}_1 \\ \hat{z}_2 \\ \hat{z}_3 \end{bmatrix} + \begin{bmatrix} 0 \\ 10 \\ 0 \end{bmatrix} \hat{u} + \begin{bmatrix} 24 \\ 192 \\ 512 \end{bmatrix} Y \tag{63}$$

$$u = \begin{bmatrix} 3.6 & 1.2 & 0.1 \end{bmatrix} \left(\begin{bmatrix} r \\ \dot{r} \\ 0 \end{bmatrix} - \begin{bmatrix} \hat{z}_1 \\ \hat{z}_2 \\ \hat{z}_3 \end{bmatrix} \right) \tag{64}$$

In this article, only the rotation angle and speed of the actuator are studied, therefore, the state vector in Eq (63) is expressed as $\begin{bmatrix} Y & \dot{Y} & e \end{bmatrix}^T$, and e refers to the external disturbance. The nonlinear dynamics of the actuator $N(\cdot)$ with reference to [25] is selected as the first-order motor model with a transfer function of 300/(s + 300). In the simulation employed in this paper, models of both the cavitator and the fin are selected as 300/(s + 300).

5.2. Simulation and verification

The parameters of the linear active disturbance rejection controller suitable for Section 5.1 are not unique. At the time of design, definition 2 and 3 are needed to help determine whether the controller design is reasonable.

Therefore, this section will use the simulation method to analyze the performance of the designed LESO and verify whether the output of the LESO can accurately track the state value of the system. It should be noted that in the simulation diagram in this section, all ordinates are test values, and these test values will have no physical units.

Figure10 is a comparison diagram of the system output y and its first derivative $\dot{y}$ with the observation value $\hat{z}$ of the linear expansion state observer and its first derivative $\dot{\hat{z}}$ when the reference input of the active disturbance rejection controller is zero.

It can be verified that when the reference input $r = 0$ and the coefficients k_i of the state feedback gain K_o are not all 0, the observation value $\hat{z}$ and its first derivative $\dot{\hat{z}}$ of the linear expansion state observer can track the output y of the system and its first derivative $\dot{y}$ very well.

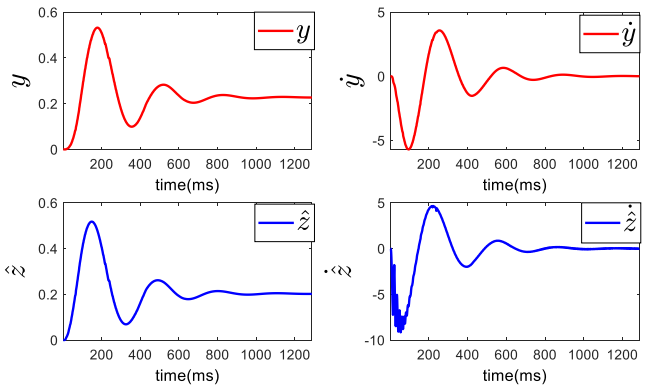

Figure 10. Output VS state observe value ($r = 0$).

This verifies the correctness of definition 2 and shows that the linear active disturbance rejection control designed in this paper is correct.

The Figures 11 and 12 are comparison diagrams of the reference input r and its first derivative $\dot{r}$ as well as the observation value $\hat{z}$ of the linear expansion state observer and its first derivative $\dot{\hat{z}}$ when the reference input of the controller is a unit step signal or a sinusoidal signal, respectively.

It can be seen from Figures 11 and 12 that when the linear expansion state observer is designed reasonably and the parameters k_i of the state feedback gain K_o are not all 0, the observation value $\hat{z}$ and its first derivative $\dot{\hat{z}}$ can track the reference input r and its first derivative $\dot{r}$ well. This verifies that definition 3 is correct, and also shows that the active disturbance rejection control designed in this paper is suitable.

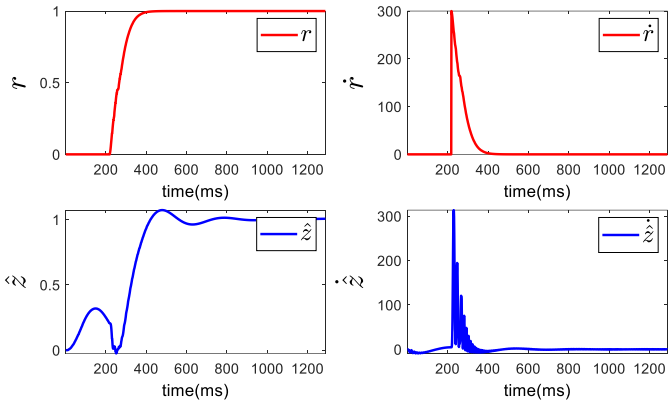

Figure 11. Input VS state observe value (r is a unit step signal).

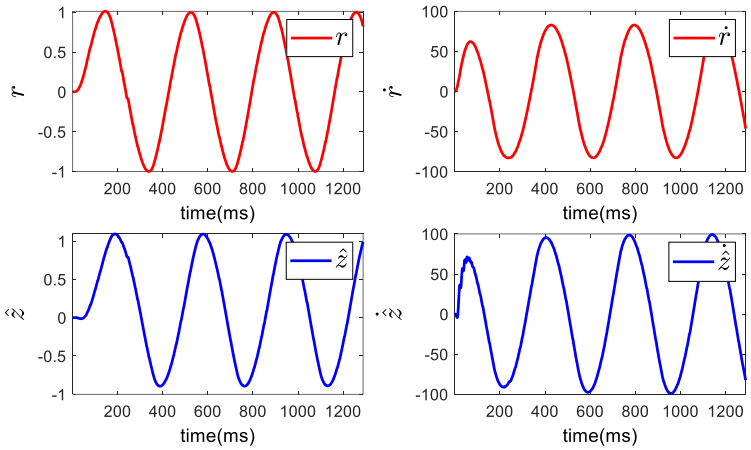

Figure 12. Input VS state observe value (r is a sinusoidal signal).

The Figures 13−15 show the motion state of the supercavitating vehicle, the rotation angle and the rotation speed of the cavitator as well as the fin, planning force, and fin immersion depth at the reference input r = 0.

Due to the influence of the additional control structure on the stable poles, the following simulation only retains the term z = 0.05 m in the original expected poles.

Figure 13 shows that under the control of LADRC, the supercavitating vehicle moves linearly with a fixed depth, and no large displacement occurs. During the motion, the fin of the vehicle is not

in contact with the cavity wall (Figure 15), therefore, the control system designed in this section is stronger in terms of stability than that of the control system designed in Section 3.1.

Since the active disturbance rejection controller provides the cavitator with an additional control value u for the vehicle. It can be seen from Figure 14 that the rotation angle and rotation speed provided the cavitator and the fin are not large. Besides, the rotation angle and rotation speed are in accordance with the allowable range in which the actual motor can work normally, therefore, the vehicle can sail stably without saturation of the actuator.

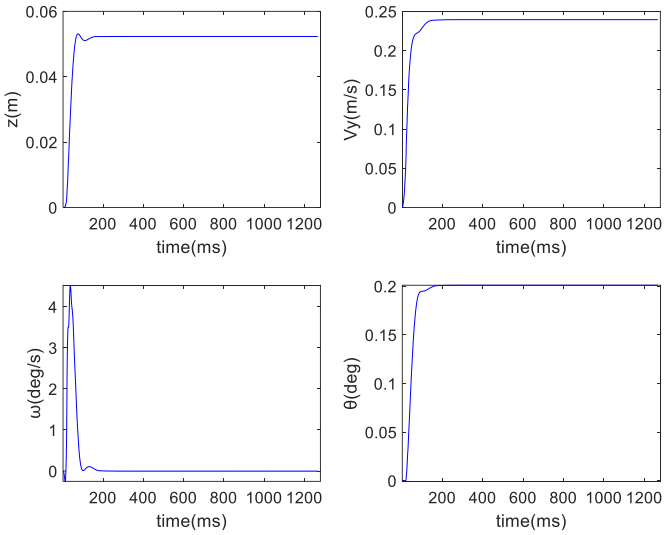

Figure 13. The motion states of HSSV (with LADRC).

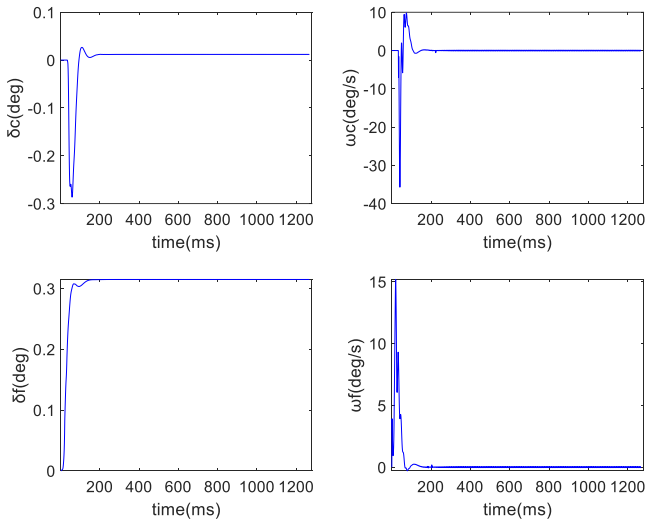

Figure 14. The degree and rotate velocity of cavitator or fin (with LADRC).

The following experiment will offer a pulse disturbance which will be added to the variable of v_y to simulate the motion state of the supercavitating vehicle with planning force, so as to observe whether the active disturbance rejection controller can maintain the stable motion of the vehicle and restrain the actuator saturation phenomenon in the presence of the planning force.

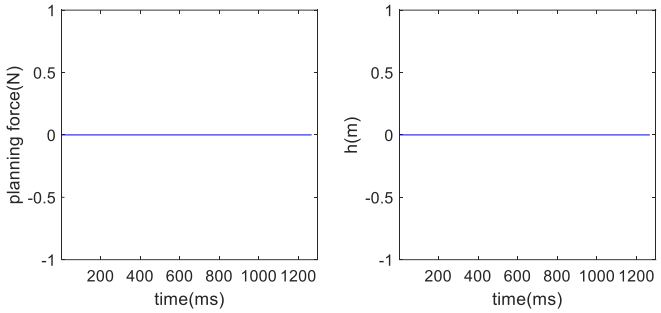

Figure 15. The planning force and immersion depth of HSSV (with LADRC).

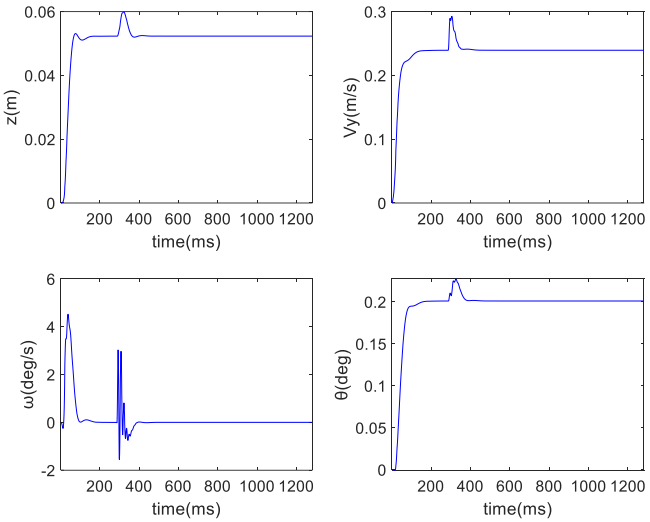

Figure 16. The motion state of HSSV.

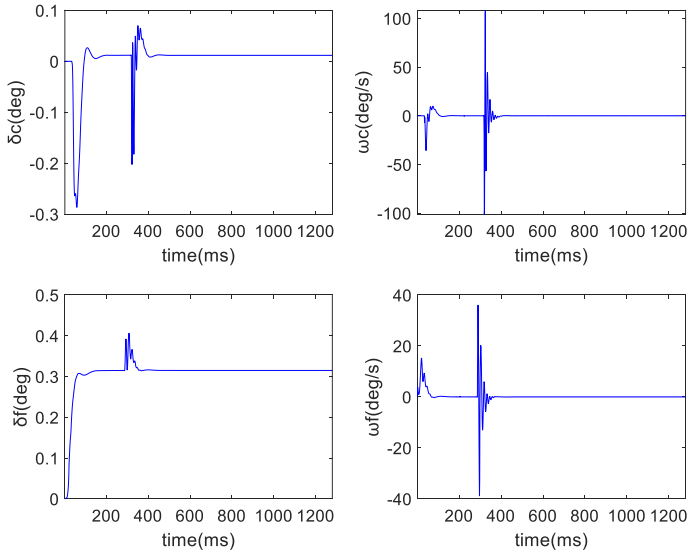

Figure 17. The degree and rotate velocity of cavitator or fin.

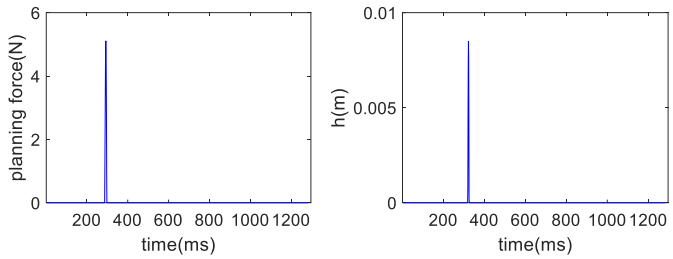

Figure 18. The planning force and immersion depth.

Due to the fact that pulse interference are provided to v_y, sudden changes occurred to the motion state of the vehicle instantaneously, and the rotation angle or rotation speed of the actuator at this moment is also the largest. Therefore, it can be seen from the above figure that the vehicle can still maintain stable movement when the pulse interference e is applied.

However, the active disturbance rejection controller introduces interference into the state $\hat{z}_3$, and mitigates the most drastic changes in the rotation angle and angular velocity of the actuator through additional control variable u from the cavitator, in that case, the active disturbance rejection controller restrains the actuator saturation phenomenon.

6. Conclusions

In this paper, firstly, by analyzing the actuator saturation problem of supercavitating vehicle in controllable motion, it is concluded that the simulation results of stable motion of supercavitating vehicle realized by general robust pole assignment control algorithm are not in line with the actual situation. Then, based on the original controller, the outer loop controller of the supercavitating vehicle is designed by using the LADRC, which provides additional control variables for the cavitator of supercavitating vehicle. Finally, the simulation results show that the LADRC can reduce the deflection angle and deflection angle speed of the actuator of the supercavitating vehicle, and ensure the stable movement of the supercavitating vehicle on the premise of preventing actuator saturation.

However, the research of this paper also has limitations, the ADRC algorithm requires that the input of LESO is an accurate value, however, the depth measurement of supercavitating vehicle has always been one of the unsolved problems. In the future, the author will conduct more in-depth research on the combination of active disturbance rejection control and motion control of supercavitating vehicle, so as to promote the development of related topics of supercavitating vehicle control.

Acknowledgments

This study was supported in part by the National Natural Science Foundation of China under Grant 51309058 and Natural Science Foundation of Heilongjiang Province under Grant LH2021E043. The authors are grateful to the editor for handling this paper and to the three anonymous referees for their helpful comments that have significantly improved this paper.

Conflict of interest

The authors declare there is no conflict of interest.

References

1. J. Dzielski, A. Kurdila, A benchmark control problem for supercavitating vehicles and an initial investigation of solution, *J. Vib. Control*, **9** (2003), 791–804. doi: 10.1177/1077546303009007004.
2. I. N. Kirschner, D. C. Kring, A. W. Stokes, N. E. Fine, J. S. Uhlman, Control strategies for supercavitating vehicles, *J. J. Vib. Control*, **8** (2002), 219–242. doi:10.1177/107754602023818.
3. V. N. Semenenko, *Artificial supercavitation, physics and calculation*, in RTO AVT lecture series on supercavitating flows, Von Karman Institute, Brussels Belgium, 2001. Available from: https://www.researchgate.net/publication/235099692.
4. R. E. A. Arndt, Cavitation in vortical flows, *Annu. Rev. Fluid Mech.*, **34** (2003), 143–175. doi: 10.1146/annurev.fluid.34.082301.114957.
5. D. E. Sanabria., G. J. Balas, R. E. A. Arndt, Modeling, control, and experimental validation of a high-speed supercavitating vehicle, *IEEE J. Oceanic Eng.*, **40** (2015), 362–373. doi: 10.1109/JOE.2014.2312591.
6. D. E. Sanabria, R. E. A. Arndt, Robust control of a small-scale supercavitating vehicle: From modeling to testing, *Ocean Eng.*, **160** (2018), 412–424. doi: 10.1016/ j. oceaneng.2018.04.060.
7. X. Yuan, T. Xing, Hydrodynamic characteristics of a supercavitating vehicle's aft body, *Ocean Eng.*, **114** (2016), 37–46. doi: 10.1016/j.oceaneng.2016.01.012.
8. L. Zhang, S. Lin, C. Wang, D. Xie, J. Sun, A new simulation model for hydrodynamic behavior of rigid body in narrow space. *Ocean Eng.*, **182** (2019), 427–441. doi: 10. 1016/ j. oceaneng.2019.04.046.
9. X. Zhang, Y. Wei, Y. Han, T. Bai, K. Ma, Design and comparison of LQR and a novel robust backstepping controller for supercavitating vehicles, *Trans. Inst. Meas. Control*, **39** (2017), 149–162. doi: 10.1177/0142331215607614.
10. Y. Shao, M. Mesbahi, G. J. Balas, Planing, switching, and supercavitating flight control, in *AIAA Guidance, Navigation, and Control Conference and Exhibit*, (2003). doi: 10.2514/6.2003-5724.
11. B. Vanek, J. Bokor, G. J. Balas, R. E. A. Arndt, Longitudinal motion control of a high-speed supercavitation vehicle, *J. Vib. Control*, **13** (2007), 159–184. doi: 10. 1177/107 7546307070226.
12. X. Mao, Q. Wang, Nonlinear control design for a supercavitating vehicle, *IEEE Trans. Contrl. Syst. Technol.*, **17** (2009), 816–832. doi: 10.1109/TCST.2009.2013338.
13. Y. Han, Z. Xu, H. Guo, Robust predictive control of a supercavitating vehicle based on time-delay characteristics and parameter uncertainty, *Ocean Eng.*, **237** (2021), 1–10. doi: 10.1016/j.oceaneng.2021.109627.
14. S. D. Escobar, G. J. Balas, R. E. A. Arndt, Planing avoidance control for supercavitating vehicles, in *2014 American Control Conference*, (2014), 4979–4984. doi: 10.1109/ACC.2014.6859485.
15. X. Zhang, Y. Han, T. Bai, Y. Wei, K. Ma, H-infinity controller design using LMIs for high-speed underwater vehicles in presence of uncertainties and disturbances, *Ocean Eng.*, **104** (2015), 359–369. doi:10.1016/j.oceaneng.2015.05.026.
16. X. Zhao, X. Ye, Sliding mode controller design for supercavitating vehicles, *Ocean Eng.*, **184** (2019), 173–183. doi: 10.1016/j.oceaneng.2019.04.066.
17. Y. Bai, J. D. Biggs, Z. Zhang, Y. Ding , Adaptive fault-tolerant control for longitudinal motion of supercavitating vehicles. *Eur. J. Control*, **57** (2021), 263–272. doi: 10.1016/j.ejcon.2020.06.002.

18. B. D. H. Phuc, S. D. Lee, S. S. You, N. S. Rathore, Nonlinear robust control of high-speed supercavitating vehicle in the vertical plane. *J. Eng. Marit. Environ.*, **234** (2019), 510−519. doi: 10.1177/1475090219875861.
19. B. Qiang, L. Zhang, Output feedback control design to enlarge the domain of attraction of a supercavitating vehicle subject to actuator saturation, in *32nd Institute of China Electronics Technology Group Corporation*, **40** (2018): 3189−3200. doi: 10.1177/0142331217718898.
20. T. Akash, S. Pushpendra, L. K. Mohan, H. Jalpa, Fuzzy logic controller and game theory based distributed energy resources allocation, *AIMS Energy*, **8** (2020), 474−492. doi: 10.3934/energy.2020.3.474.
21. I. Katherin, L. W. Bambang, M. Ali, Intelligent distribution network design of sensor and actuator fault tolerant control system on wind turbine benchmark for Region II, *AIMS Energy*, **7** (2019), 111–126. doi: 10.3934/ENERGY.2019.2.111.
22. T. S. S Senarathna, K. T. M Udayanga Hemapala, Review of adaptive protection methods for microgrids, *AIMS Energy*, **7** (2019): 557–578. doi: 10.3934/energy.2019.5.557.
23. X. Le, J. Wang, Robust pole assignment for synthesizing feedback control systems using recurrent neural networks, *IEEE Trans. Neural. Netw. Learn. Syst*, **25** (2014), 383–393. doi: 10.1109/TNNLS.2013.2275732.
24. B. Ralph, G. Stephen, Approaches to robust pole assignment, *Int. J. Control*, **49** (1989), 97–117. doi: 10.1080/00207178908559623.
25. J. B. Correction, X. Luo, R. E. A. Arndt, Y. Wu, Numerical simulation of three dimensional cavitation shedding dynamics with special emphasis on cavitation-vortex interaction, *Ocean Eng.*, **87** (2014), 64–77. doi:10.1016/j. oceaneng.2014.05.005.
26. X. Long , H. Cheng , B. Ji , R. E. A. Arndt, X. Peng, Large eddy simulation and Euler-Lagrangian coupling investigation of the transient cavitating turbulent flow around a twisted hydrofoil, *Int. J. Multiphase Flow*, **100** (2018): 41–56. doi: 10.1016/j.ijmultiphaseflow.2017.12.002.
27. A. Karn , R. E. A. Arndt, J. Hong, Gas entrainment behaviors in the formation and collapse of a ventilated supercavity, *Exp. Therm. Fluid Sci.*, **79** (2016), 294–300. doi: 10.1016/j.expthermflusci.2016.08.003.
28. W. Zou, H. Liu, L. Xue, Three-dimensional ventilated supercavity on a maneuvering trajectory, *Ocean Eng.*, **122** (2016), 97–104. doi:10.1016/j. oceaneng.2016.06.023.
29. S. Shao, Y. Wu, J. Haynes, R. E. A. Arndt, J .Hong, Investigation into the behaviors of ventilated supercavities in unsteady flow, *Phys. Fluids*, **30** (2018), 236–241. doi:10.1063/1.5027629.
30. M. Murayama, Y. Yoshida, Y. Tsujimoto, Unsteady tip leakage vortex cavitation originating from the tip clearance of an oscillating hydrofoil, *J. Fluids Eng.*, **128** (2006), 421–429. doi:10.1115/1.2173290.
31. A. Karn, R. E. Arndt, J. Hong, An experimental investigation into supercavity closure mechanisms, *J. Fluid Mech.*, **789** (2016), 259–284. doi:10.1017/jfm.2015.680.